Enzymatic biomineralization of biocompatible $CuInS_2$, $(CuInZn)S_2$ and $CuInS_2$/ZnS core/shell nanocrystals for bioimaging†

Leah C. Spangler,[a] Roxanne Chu,[a] Li Lu,[b] Christopher J. Kiely,[a,b] Bryan W. Berger*[a,c] and Steven McIntosh*[a]

This work demonstrates a bioenabled fully aqueous phase and room temperature route to the synthesis of $CuInS_2$/ZnS core/shell quantum confined nanocrystals conjugated to IgG antibodies and used for fluorescent tagging of THP-1 leukemia cells. This elegant, straightforward and green approach avoids the use of solvents, high temperatures and the necessity to phase transfer the nanocrystals prior to appli-cation. Non-toxic $CuInS_2$, $(CuInZn)S_2$, and $CuInS_2$/ZnS core/shell quantum confined nanocrystals are synthesized via a biomineralization process based on a single recombinant cystathionine γ-lyase (CSE) enzyme. First, soluble In–S complexes are formed from indium acetate and H_2S generated by CSE, which are then stabilized by L-cysteine in solution. The subsequent addition of copper, or both copper and zinc, precursors then results in the immediate formation of $CuInS_2$ or $(CuInZn)S_2$ quantum dots. Shell growth is realized through subsequent introduction of Zn acetate to the preformed core nanocrystals. The size and optical properties of the nanocrystals are tuned by adjusting the indium precursor concentration and initial incubation period. $CuInS_2$/ZnS core/shell particles are conjugated to IgG antibodies using EDC/NHS cross-linkers and then applied in the bioimaging of THP-1 cells. Cytotoxicity tests confirm that $CuInS_2$/ ZnS core/shell quantum dots do not cause cell death during bioimaging. Thus, this biomineralization enabled approach provides a facile, low temperature route for the fully aqueous synthesis of non-toxic $CuInS_2$/ZnS quantum dots, which are ideal for use in bioimaging applications.

Introduction

Perhaps the primary biomedical application of quantum con-fined semiconductor nanocrystals is as fluorescent markers in cellular labeling and bioimaging. Quantum dots are con-sidered superior to traditional fluorescent dyes due to their good photo-stability, high quantum yields, and long fluo-rescent lifetimes.[1,2] Furthermore, a wide range of emission wavelengths across the visible and infrared regions are accessi-ble by tuning the size or composition of the nanocrystal.[3] Additionally, quantum dots of the same material, but with different sizes, provide a range of different fluorescence wavelengths that can be illuminated using the same energy excitation source. This is especially desirable for simultaneous tagging and identification of different areas or processes within a single cell.[4,5]

To be fully compatible with in vivo biological systems, the nanocrystals must be non-toxic, stable in water at physiological pH, and readily conjugated to a selective biomarker such as an antibody or antigen that binds to a specific receptor on the target cells.[2,6] While cadmium based materials are widely reported for in vitro applications, their potential toxicity has prompted research into alternative, non-toxic compositions.[7,8] $CuInS_2$ is a non-toxic semiconductor material that fluoresces in the visible range, in a similar manner to CdS.[9] While $CuInS_2$ quantum dots typically have low fluorescence as syn-thesized, coating or alloying them with ZnS has been reported to improve their quantum yield, up to 80% in some cases.[10–13]

The requirement for aqueous phase stability at physiologi-cal pH is in stark contrast to the typical high temperature organic phase quantum dot synthesis procedures. While these routes lead to high yields of good quality materials, utilization of an organic based synthesis route requires additional proces-sing to transfer the nanocrystals into the aqueous phase using either ligand exchange or encapsulation in a polymer shell or

[a]Department of Chemical and Biomolecular Engineering, Lehigh University, Bethlehem, PA 18015, USA. E-mail: mcintosh@lehigh.edu, berger@lehigh.edu
[b]Department of Materials Science and Engineering, Lehigh University, Bethlehem, PA 18015, USA
[c]Program in Bioengineering, Lehigh University, Bethlehem, PA 18015, USA
† Electronic supplementary information (ESI) available. See DOI: 10.1039/ c7nr02852k

micelle.[2,3,6] Furthermore, these organic syntheses procedures often utilize toxic precursors which could cause contamination in the final product.[14] All of these factors have motivated our research towards developing an aqueous based synthesis route for biocompatible quantum confined $CuInS_2$ nanocrystals.

Several groups have been investigating the aqueous chemi-cal synthesis of quantum dots to avoid an additional phase transfer step.[15] While there has been some success, many of these techniques still require high temperatures and/or press-ures to generate crystalline particles. This requirement increases cost and limits potential scale-up for use in indus-trial biomedical applications.

There are many proposed aqueous synthesis routes for $CuInS_2$ based quantum dots. The most common procedure described is the hydrothermal method, performed in an auto-clave at 100–150 °C and at pH 11 or higher.[16–18] Typically, chloride salts of copper and indium are used in addition to a reactive sulfur precursor such as thiourea or Na_2S. In a few cases, $(CuInZn)S_2$ quaternary alloys have been formed by also adding zinc acetate or zinc chloride.[19,20] Commonly used capping agents include MPA, glutathione, and L-cysteine. Many groups have successfully applied the resulting materials for bioimaging of cancer cells. Xiong et al. have utilized similar precursors and reaction conditions, but eliminated the need for high pressure conditions by heating to 100 °C using microwave irradiation.[21] Additionally, a ZnS shell is frequently grown on these materials to improve the fluorescence pro-perties of the nanocrystals. The resulting glutathione capped $CuInS_2$/ZnS core/shell quantum dots are used without conju-gation for cell labeling, or conjugated to an antibody for a fluoroimmunoassay that can be used for early detection of cancer. Chen et al. demonstrated another open-air procedure to synthesize glutathione capped $CuInS_2$/ZnS core/shell nano-crystals.[22] Copper and indium salts were heated at 95 °C with Na_2S as a reactive sulfur precursor to form $CuInS_2$ nanocrys-tals, and subsequent growth of a ZnS shell was achieved by further heating the solution in the presence of zinc acetate and thiourea.

Wang et al. have proposed that significant energy and environmental cost savings can be achieved by greener nano-crystal synthesis that can occur at ambient temperature without a harsh chemical environment.[23] The aqueous syn-thesis approach they describe occurs at, or below, room temp-erature at a pH of 7.4 utilizing copper sulfate, indium chloride, thioacetamide as sulfur source, and the protein bovine serum albumin (BSA) as a capping agent. While this approach formed nanocrystals, no photoluminescence was reported and the synthesis procedure required about 100 h to complete, most likely due to the slow decomposition rate of the thio-acetamide. This long synthesis time negatively impacts the potential economics of the production route and is a common criticism of green approaches to nanoparticle synthesis. In the absence of elevated temperature, pH or direct addition of a reactive chemical precursor, an additional driving force is required to achieve aqueous phase nanocrystal formation under ambient conditions at shorter timescales.

Herein we have drawn inspiration from biological systems, and demonstrate the single enzyme catalyzed biomineral-ization of quantum confined $CuInS_2$, $(CuInZn)S_2$ and $CuInS_2$/ ZnS core/shell nanocrystals and demonstrate their efficacy in the bioimaging of THP-1 leukemia cells. Biomineralization is the process whereby biological systems mineralize inorganic materials.[24] In contrast to bio-inspired approaches that typi-cally utilize a biomolecule to template chemically induced mineralization,[25–27] we have recently developed a single-enzyme based approach that enables direct biomineralization of aqueous stable quantum confined nanocrystals from the fewest possible components at ambient temperature.[28] Mineralization is catalyzed in otherwise inert solutions by the enzymatic turnover of the amino acid L-cysteine to form reactive H_2S as a sulfur source which then reacts with metal salts in solution. The L-cysteine serves a dual role as sulfur source and capping agent. We have previously demonstrated this approach for non-biocompatible materials such as CdS and CdSe.[28,29] In this current work, we demonstrate the biomineralization of non-toxic, biocompatible $CuInS_2$, $(CuInZn)S_2$ and $CuInS_2$/ZnS quantum dots for bioimaging applications.

Experimental

CSE was overexpressed and purified from recombinant E. coli cells, as reported previously.[28] Briefly, E. coli was grown to sat-uration at 37 °C and then diluted to an initial OD_{600} of 0.8. Expression was induced using 1 mM IPTG and performed for 16 h at 20 °C. After expression, the cells were harvested using centrifugation at 3000g, re-suspended in lysis buffer (10 mM imidazole, 100 mM HEPES, 500 mM NaCl, 10% glycerol), and sonicated at 12 W for 10 seconds on/10 seconds off at 4 °C. This cell lysate was centrifuged at 8500 rpm to purify the supernatant containing the recombinant CSE. The supernatant was then further purified using immobilized metal affinity chromatography (IMAC). The IMAC column contained Ni-NTA chelating sepharose (GE Healthcare) and the cell lysate was eluted using increasing concentrations of imidazole buffer (20 mM HEPES, 500 mM NaCl, 10% glycerol, and 10–500 mM imidazole). The CSE was stored in imidazole buffer until use.

$CuInS_2$ nanocrystal growth was performed by incubating indium nitrate (4 mM, Alfa Aesar Puratronic), L-cysteine (16 or 32 mM, Spectrum Chemicals, 99.55%), and CSE (0.1 mg mL^{-1} or 0.2 mg mL^{-1}) in Tris-HCl buffer (0.1 M, pH 7.5) for 2–6 h at 37 °C. After verifying the presence of a 290 nm peak in the absorbance spectrum, which indicates the formation of <1 nm indium sulfide complexes, copper acetate (2 mM, Alfa Aesar Puratronic, 99.99%) was added to the solution. The solution immediately turned yellow, orange, or red, depending on the size of the nanocrystals formed. Subsequent shell growth was performed by adding zinc acetate (2 or 4 mM, Alfa Aesar Puratronic) to the $CuInS_2$ sol after 1 h of incubation at room temperature. The sols were then left to incubate at room temp-erature for 1–16 h.

$(CuInZn)S_2$ quaternary alloy quantum dots were synthesized in a similar manner to the $CuInS_2$ nanocrystals. Indium nitrate (4 mM) was incubated with L-cysteine (32 mM) and CSE (0.2 mg mL^{-1}) for 4 or 6 h. Then, copper acetate (2 mM) and zinc acetate (4 mM) were added simultaneously to the solu-tion, resulting in an instantaneous color change from clear to yellow.

The biosynthesized nanocrystals were analyzed without any further purification steps. Optical absorbance measurements were performed using a UV-Vis 2600 spectrophotometer equipped with an ISR-2600-Plus integrating sphere attachment (Shimadzu). Photoluminescence spectra were obtained using a QuantaMaster™ 400 (Photon Technology International) or a Fluorolog-3 spectrofluorometer (Horiba). Photoluminescence lifetime measurements were obtained using the Fluorolog-3 spectrofluorometer with attached Time-Correlated Single Photon Counting (TCSPC) controller. The excitation source was a 478 nm laser (Delta Diode). The photoluminescence life-times were calculated from the decay curves using a bi-expo-nential fit. Quantum yield (QY) values were determined using the reference dye Coumarin 153 in ethanol.[30]

Samples used for transmission electron microscopy analysis were first diluted 100× in DI water. Next, a single drop was dis-persed onto a holey carbon coated Ni or Au-mesh grid and the liquid allowed to evaporate at room temperature in a vacuum overnight. The samples were then analyzed using an aberra-tion corrected JEOL ARM 200CF analytical electron microscope operating at 200 kV equipped with a JEOL Centurio X-ray energy dispersive spectroscopy (XEDS) system. Samples used for XEDS analysis in the scanning electron microscope were precipitated from aqueous solutions using ethanol three times and then dispersed on a glass microscope slide to dry. The dried powder was then mounted onto conductive carbon tape and imaged using a Zeiss 1550 FEG-SEM equipped with an Oxford Instruments XEDS detector.

Quantum dot–antibody conjugates were formed using 1-ethyl-3-(3-dimethylaminopropyl) carbodiimide hydrochloride (EDC) and N-hydroxysulfosuccinimide (NHS) cross-linkers,[31] obtained from Thermo Fisher Scientific. Prior to conjugation, the quantum dots were buffer exchanged from Tris-HCl to phosphate buffered saline (PBS, 10 mM) using successive concentration and re-suspension via centrifugation filters (9 K, Thermo Fisher Scientific). 10 μL of an EDC solution (20 mg mL^{-1}, Thermo Fisher Scientific) and 1 μL of NHS (20 mg mL^{-1}, Thermo Fisher Scientific) were added to 100 μL of a con-centrated $CuInS_2$/ZnS quantum dot solution. The EDC solution was prepared immediately prior to use to prevent hydrolysis. The solutions were briefly centrifuged to remove any precipi-tated nanocrystals and then 100 μL of 151-IgG (specific for epi-dermal growth factor receptor; EGF receptor) was added to the solution (DSHB Hybridoma Product 151-IgG or 151-8 AE4).[32] The quantum dot bioconjugate solutions were then incubated for 1 h at 37 °C.

THP-1 cells were maintained at 37 °C under 5% CO_2 in RPMI 1640 medium containing 10% FBS. The cells were grown to confluence and then 50 μL of either the buffer exchanged quantum dots or the quantum dot–antibody mixture were added to 300 μL of the cell solution. THP-1 cells were de-posited onto ibiTreat μ-Dishes (Ibidi, Martinsried, Germany), treated with poly-L-lysine. These cells were then incubated at 37 °C for 3 h. The cells were washed twice with PBS buffer prior to optical microscopy analysis.[31] The μ-Dish, containing the THP-1 cells and quantum dot antibody mixture, was imaged using a Nikon C2si+ confocal microscope equipped with a LU-N4S laser unit and a 40× air objective (NA = 0.95). The images were processed using Elements version 4.3 (Nikon) and Fiji. To check for cell viability in the presence of quantum dots, a Trypan blue assay was used to determine the quantity of living cells every 20 minutes over a period of 6 h.[33] The approximate cell seeding density employed was 4.5×10^5 cells per mL. Cell viability remained at or above 95% over the entire time-period.

Results

Incubation of CSE with a buffered solution of copper acetate leads to the appearance of an optical absorption onset at ~700 nm, which is in agreement with that expected for the for-mation of $Cu_{2-x}S$ nanocrystals, Fig. 1(a). This process is similar to the biomineralization of CdS and PbS as previously reported by our group.[28,34–36] Mineralization occurs as H_2S is generated by the enzymatic turnover of L-cysteine by CSE. This H_2S then reacts with the metal salt in solution to form the metal sulfide. This process is analogous to the chemical route to aqueous phase sulfide mineralization whereby reactive Na_2S is added to induce mineralization of, for example, $Cu_{2-x}S$.[37] The formation of nanoparticles, as opposed to bulk materials,
is due to (i) the presence of the L-cysteine which can act as a capping agent,[38,39] and (ii) the templating ability of the CSE enzyme itself.[28] Unfortunately, no corresponding fluorescence peak could be observed due to a very low fluorescence inten-sity. This is a common issue with $Cu_{2-x}S$ nanocrystals, and is typically attributed to oxidation of as-synthesized stoichio-metric Cu_2S nanocrystals to form non-fluorescing non-stoi-chiometric $Cu_{2-x}S$. Hence, fluorescence data for these $Cu_{2-x}S$ materials is rarely reported. To our knowledge, only two groups have reported such data for $Cu_{2-x}S$ materials which were synthesized under strictly oxygen free conditions.[40,41]

Similar incubation of CSE in a buffered solution of indium nitrate leads to the appearance of an absorbance peak centered at 290 nm that grows in intensity with increasing incubation time, Fig. 1(b). A peak at the same position is observed when indium and Na_2S are combined in the presence of L-cysteine, Fig. S1.† When L-cysteine is not present in solution, a cloudy solution forms with no strong peak at 290 nm. This suggests the formation of bulk indium sulfide and indium hydroxide precipitates, which occur at neutral and basic pH.[42] The peak position at 290 nm is in agreement with prior reports and is due to the formation of small (<1 nm) molecular indium sulfide clusters.[43–46] No shift in the absorbance spectra was observed, indicating that the clusters remain the same size

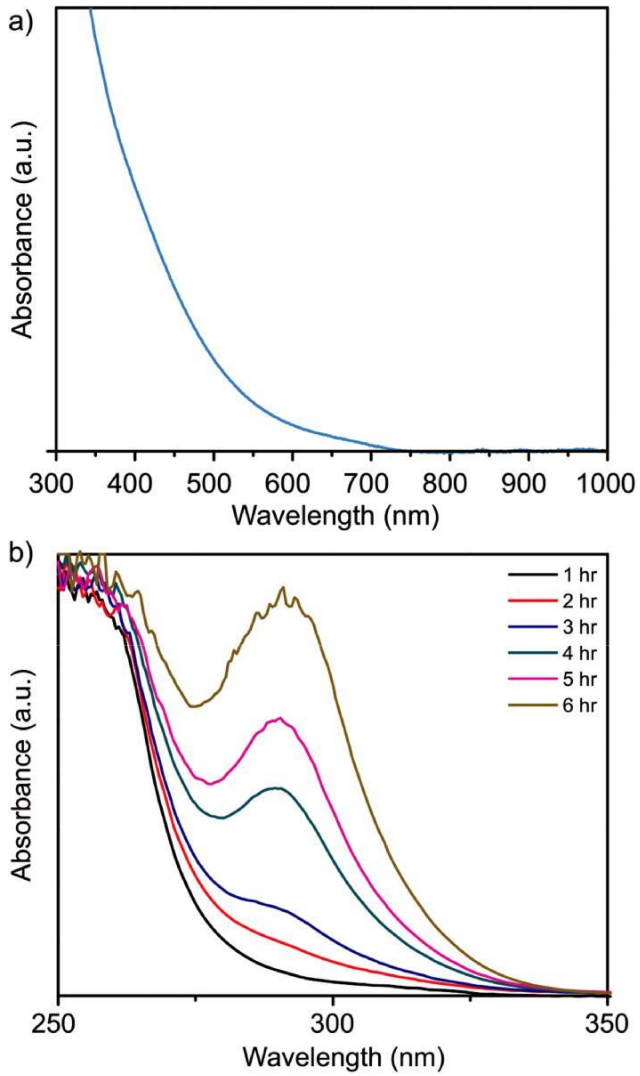

Fig. 1 Absorbance spectra of (a) $Cu_{2-x}S$ nanocrystals and (b) In–S complex solutions as a function of time when synthesized by incubation of CSE, L-cysteine and copper acetate or indium nitrate, respectively.

over the incubation period. The growth in intensity of this peak with synthesis time is indicative of an increasing concen-tration of these clusters, formed as the enzyme turns over more of the L-cysteine to form H_2S. In support of this concept, doubling the concentration of L-cysteine and CSE was found to increase the rate of growth in peak intensity, see Fig. S2,† demonstrating an increased synthesis rate of the molecular clusters. Therefore, while reaction with transition metals leads to the formation of solid precipitates,[47] reaction with indium leads to the formation of ultra-small soluble clusters.

The addition of 2 mM copper acetate to solutions contain-ing these biomineralized In–S clusters leads to an immediate change in solution color to yellow, orange or red, Fig. 2(a). Both the solution color and absorbance spectra, Fig. 2(b), are consistent with the formation of $CuInS_2$ nanocrystals, agreeing with previously reported data for $CuInS_2$ formed by chemical synthesis routes.[9,48–51] The sequential method of synthesis is

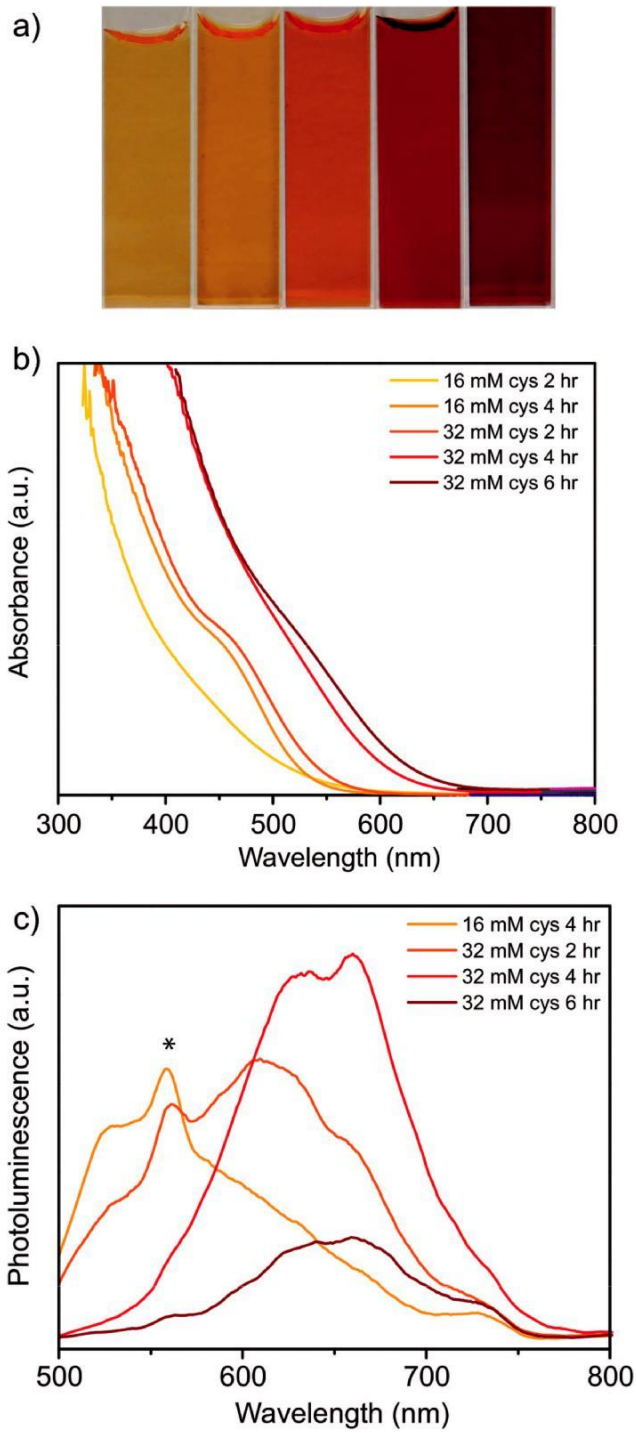

Fig. 2 (a) Photographs of solutions upon addition of 2 mM Cu acetate to solutions of CSE, L-cysteine and indium nitrate previously incubated for the time-period indicated and with the specified cysteine precursor concentrations. The corresponding absorbance and photoluminescence spectra of this set of materials are shown in (b) and (c) respectively. The * in (c) denotes the Raman peak of water which is not part of the quantum dot fluorescence.

required in order to prevent the nucleation of a secondary population of $Cu_{2-x}S$ nanoparticles, shown by the altered absorbance peak shape and formation of a brown solution

(Fig. S3†). The absorbance peak of the $CuInS_2$ quantum dot solutions was found to shift to longer wavelength positions with increasing incubation time and increasing L-cysteine con-centration in the original indium containing solution. The shift in absorption peak wavelength is indicative of larger par-ticles forming with increasing In–S precursor concentration. The band gap values for each solution shown in Fig. 2 were cal-culated using a Tauc plot and range from 2.35 to 1.93 eV, Table S1.† These band gap values indicate the formation of quantum confined nanocrystals with band gap values above 1.53 eV, which is the reported bulk band gap of $CuInS_2$.

The fluorescence from these samples is low (Fig. 2c), most likely suppressed due to the presence of surface defects result-ing from the low temperature, aqueous synthesis.[22] For crystal-line nanoparticles synthesized with 16 mM cysteine, photo-luminescence peaks were obscured by fluorescence from the enzyme. However, a small shoulder could be identified at around ~600 nm in Fig. 2(c) for the case of a 4 h indium incu-bation. Solutions synthesized with 32 mM cysteine exhibit photoluminescence peaks shifting from 615 nm to 650 nm after 2 or 4 h indium incubation, respectively. After 6 h indium incubation, the photoluminescence peak no longer shifts but appears to decrease in intensity. This suggests the maximum number of In–S complexes has been generated in solution after 4 h In incubation, so larger crystals are no longer able to form.

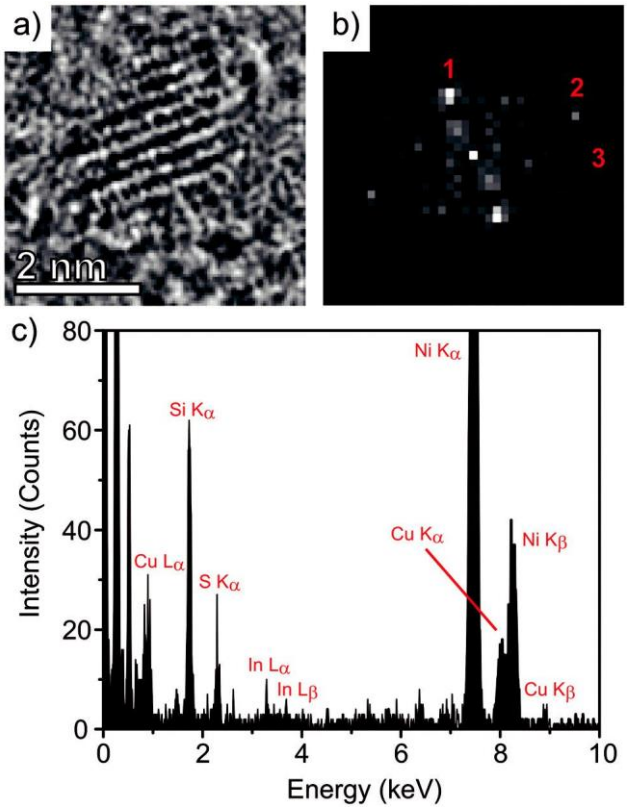

Fig. 3 (a) HRTEM phase contrast image and (b) the corresponding FFT of a single 2.5 nm $CuInS_2$ nanocrystal. Fitting of the interplanar spacings and angles of the planes in the FFT are reported in Table S2† and are consistent with the chalcopyrite crystal structure viewed along [$10\bar{3}$]. (c) Single particle STEM-XEDS analysis confirms the co-existence of Cu, In, and S within the particle.

Some groups have also reported that changes in the rela-tive Cu and In compositions (as well as size) can cause shifts in the optical spectra of $CuInS_2$ quantum dots.[52–54] Quantitative SEM-XEDS analysis was utilized to determine the compositions of quantum dots for three different indium incubation times. For $CuInS_2$ solutions made with 16 mM cysteine and 4 h In incubation time, the Cu/In ratio was 1.6 ± 0.09. When 32 mM cysteine was used with In incubation times of 4 or 6 h, the Cu/In ratios were found to be 0.7 ± 0.04 and 0.6 ± 0.04, respectively. As previously shown in Fig. 1(b) and S2,† a lower concentration of cysteine decreases the number of In–S complexes; therefore, a higher Cu/In ratio is expected for the 16 mM cysteine sample. When more In–S complexes are present, (as in the latter two samples) the $CuInS_2$ nanocrystals appear to be Cu deficient. Typically, such Cu deficient $CuInS_2$ nanocrystals have blue-shifted optical properties. As our nanocrystal solutions prepared with

32 mM cysteine continue to show a red-shift in absorbance properties relative to the 16 mM sample, we believe the change in optical properties noted is being dominated by
competing quantum confinement effects arising from par-ticle size variations.[50,55]

Fig. 3(a) shows an HRTEM phase contrast image of a repre-sentative $CuInS_2$ nanocrystal from the 32 mM cysteine, 4 h In incubation specimen shown in Fig. 2(b). A corresponding lower magnification HRTEM image showing a larger sampling of these nanocrystals is presented in Fig. S4.† The nanocrystal diameter is approximately 2.5 nm, which suggests that the quantum dot solutions should have a photoluminescence peak at ~650 nm when compared to literature reports for chemically synthesized quantum confined $CuInS_2$ nanocrystals with a Cu/In ratio of 0.7.[49] As expected, the optical properties of our material are blue-shifted from chemically synthesized nanocrystals of 2.7 nm mean diameter and 1 : 1 Cu : In stoi-chiometry, which are reported to have a photoluminescence peak at around 700 nm.[55] The corresponding fast Fourier transform (FFT) derived from Fig. 3(a) and shown in Fig. 3(b) can be indexed to the [$10\bar{3}$] projection of the chalcopyrite struc-ture of $CuInS_2$, Table S2.† A representative X-ray energy disper-sive spectrum (STEM-XEDS) from an isolated particle, Fig. 3(c), confirms the co-existence of indium, copper, and sulfur within a single particle. The copper peaks have a slight overlap with Ni, which is present from the TEM support grid. HRTEM phase contrast images of nanocrystals formed from a solution of 4 mM indium, 16 mM L-cysteine, 0.1 mg mL^{-1} CSE for 4 h initial indium show even smaller, ~2 nm particles (Fig. S5†). Again, the corresponding photoluminescence peak at ~600 nm is consistent with those reported for 2 nm chemically synthesized particles of similar composition.[22]

Many groups have shown that the growth of a ZnS shell on $CuInS_2$ quantum dots significantly increases the quantum yield. We have previously reported biomineralization of PbS/ CdS core/shell particles through the sequential addition of pre-

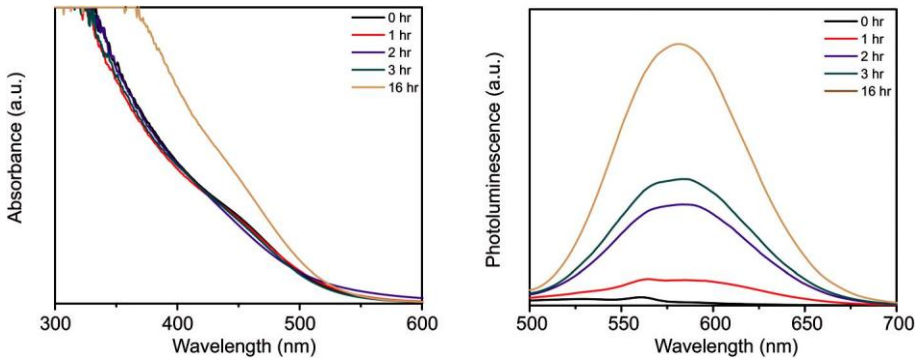

Fig. 4 Absorbance and photoluminescence spectra of $CuInS_2$/ZnS core/shell nanocrystals grown with increasing incubation time at room temperature.

cursors.[34] Incubation of CSE in a buffered solution of zinc acetate and L-cysteine leads to the formation of an absorption peak at 280 nm, Fig. S6,† in agreement with reports of ZnS nanoparticle formation.[56–58] As such, we adapted our pre-viously demonstrated procedure to incubate $CuInS_2$ core nano-particles in a buffered zinc acetate solution with L-cysteine and CSE. Fig. 4 shows the absorbance and photoluminescence spectra of the resulting material as a function of increasing incubation time with zinc acetate. Although the absorbance spectrum remains essentially unchanged except at the longest growth time, the photoluminescence properties improve dra-matically over time. The photoluminescence peak slightly blue shifts relative to that of the core $CuInS_2$ nanocrystals, indicat-ing the growth of a ZnS shell. Although core/shell quantum dots typically have photoluminescence spectra which are red-shifted from the core nanocrystals, many groups report a blue shift with $CuInS_2$/ZnS core/shell quantum dots and attribute this to a slight etching of the $CuInS_2$ core size during shell growth.[13,55] The quantum yield of the as synthesized $CuInS_2$/ZnS quantum dots was determined to be approximately 0.1% relative to the standard dye Coumarin 153 in ethanol. While this quantum yield is low compared to previous reports of $CuInS_2$/ZnS prepared in the aqueous phase,[22] these latter methods required high temperature and/or pressure to form the nanocrystals. Poor photoluminescence quantum yields are commonly found for biomineralized quantum dots made at low temperatures, and ongoing work is focused on further improving the overall quantum yield while retaining the appli-cation advantages of an aqueous synthesis procedure that operates under ambient conditions.

Fig. 5(a and b) shows some representative HRTEM phase contrast images of the biomineralized $CuInS_2$/ZnS core/shell nanocrystals. A lower magnification image is shown in Fig. S7.† The crystals are approximately 4 nm in diameter, which is larger than the typical corresponding core nanocrystal shown in Fig. 2(a). The lattice spacings and interplanar angles derived from the corresponding FFT's for both particles, Fig. 5 (c and d), can be assigned to the [010] projection of chalco-pyrite structure of $CuInS_2$, Table S3.† Based on the measured photoluminescence maxima of 630 nm for this material, we would expect the $CuInS_2$ core of these nanocrystals to be approximately 2–2.5 nm.[55,59] Assuming no intermixing of the core and shell materials, the increased overall size of the observed quantum dots suggests the growth of a ~0.75 nm thick ZnS shell on a ~2.5 nm diameter core. The lattice para-meter for sphalerite ZnS is 0.58 nm, suggesting the growth of ~1.5 monolayers. The growth of an epitaxial shell is consistent with previous reports of chemically synthesized $CuInS_2$/ZnS core/shell particles[12,13] and is expected for this system because $CuInS_2$ and ZnS (the sphalerite form) have a lattice mismatch which is less than 2%.[11] Single particle STEM-XEDS analysis, Fig. 5(e), confirms the co-existence of copper, indium, sulfur and zinc within individual particles. It was not possible using either HRTEM phase contrast or HAADF-STEM imaging modes to see a direct contrast difference between the core and shell material in this materials system.

The average composition of the same $CuInS_2$/ZnS core/shell particle preparation shown in Fig. 5 was analyzed using SEM-EDS. The Cu/In ratio was found to be 1.46 ± 0.18 (as com-pared the core material which had a Cu/In ratio of 0.7 ± 0.04) and the Zn/In ratio was 2.3 ± 0.29. The increase in Cu/In ratio relative to the starting core material suggests that the zinc is preferentially substituting for indium cations in the crystal lattice, as no additional copper was added to the solution during ZnS shell growth. This decrease of indium has also been reported by Chen et al., who also utilized an aqueous syn-thesis method in open air. In a similar manner to our system, they observed a reduction of indium content for $CuInS_2$/ZnS core/shell nanocrystals that have Cu/In ratios of less than 1 in the starting $CuInS_2$ core quantum dots.[22]

Several groups have also reported that the mixed quaternary $(CuInZn)S_2$ alloy shows improved photoluminescence pro-perties over $CuInS_2$ nanocrystals.[19,60,61] To determine whether biomineralization with CSE was capable of producing a qua-ternary alloy, we simultaneously added zinc acetate and copper acetate to a solution of 4 mM indium acetate, 32 mM L-cysteine, and 0.2 mg mL^{-1} CSE which had been incubated for 4 hours. Fig. 6 shows images, absorbance spectra, and photoluminescence spectra of the resulting 'quaternary' sols compared to that for sols of $CuInS_2$ and sequentially prepared

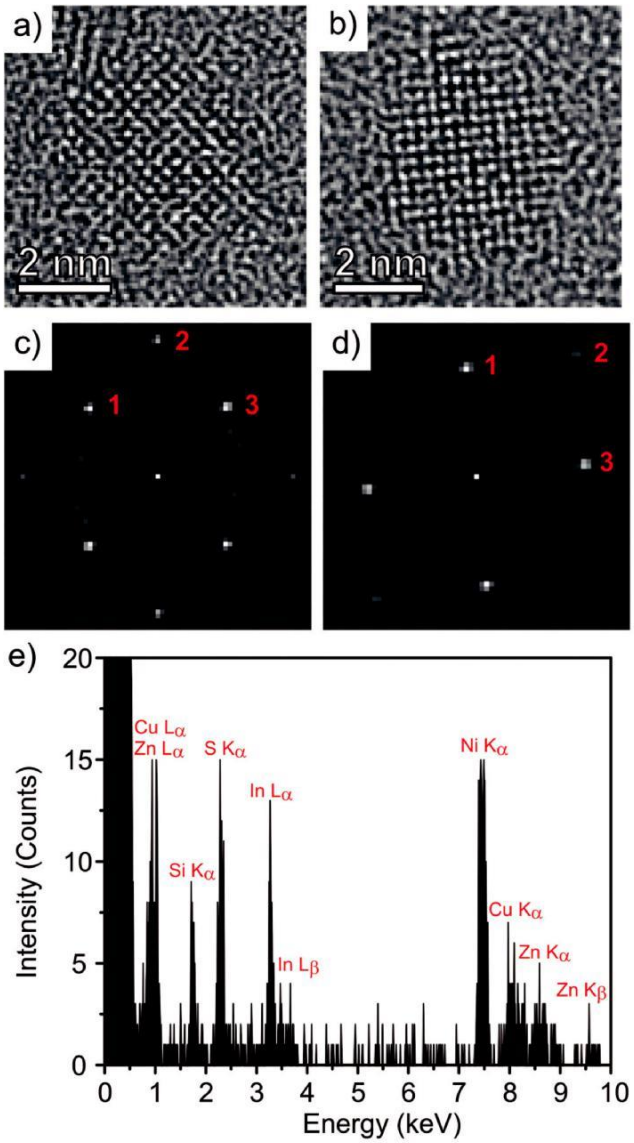

Fig. 5 (a, b) HRTEM phase contrast images and (c, d) the corresponding FFT's of 4 nm $CuInS_2$/ZnS nanocrystals with cores grown with 32 mM cys, 4 h In incubation time and Zn acetate in solution for 12 h viewed along the [010] projection. Lattice fitting of the planes in the FFT are presented in Table S3.† (e) Representative STEM-XEDS spectrum showing the co-existence of Cu, In, S, and Zn within a single particle.

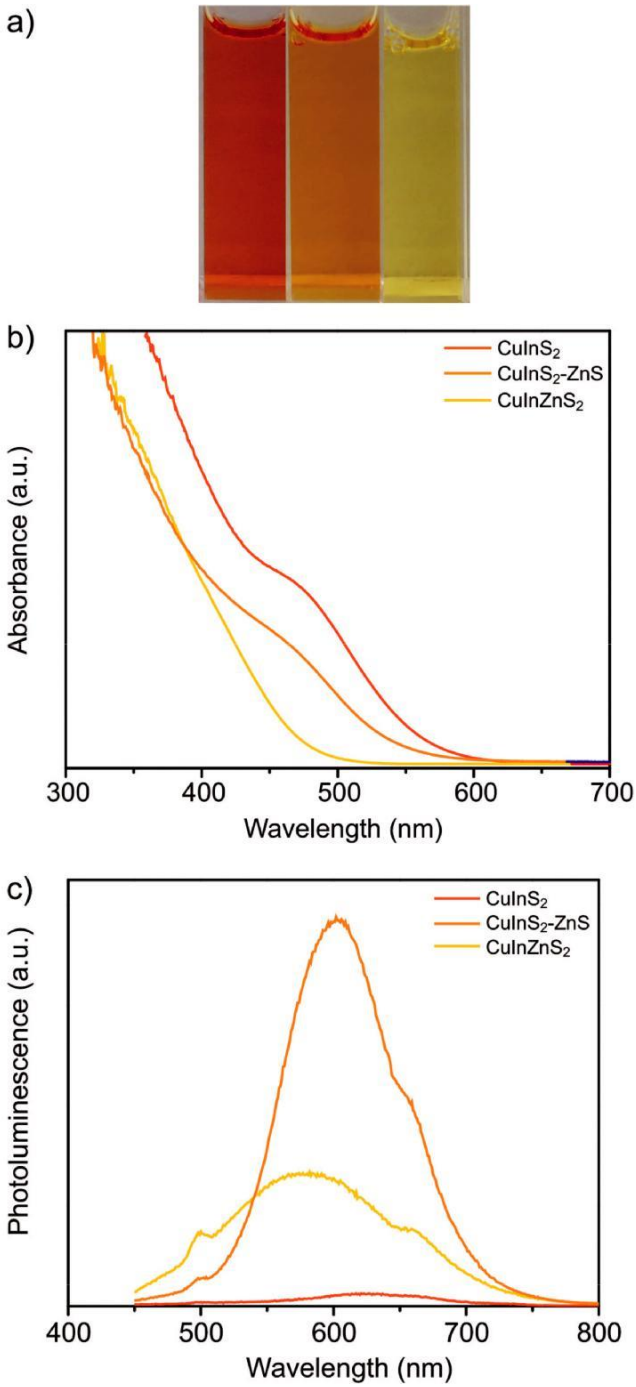

Fig. 6 (a) Images, (b) absorbance spectra, and (c) photoluminescence spectra showing the difference between the original $CuInS_2$ quantum dot sol and those materials synthesized with sequential addition versus simultaneous addition of Cu and Zn precursors leading to the formation of a $CuInS_2$/ZnS core/shell morphology or a $(CuInZn)S_2$ random alloy, respectively.

$CuInS_2$/ZnS core/shell nanoparticles. The absorbance and fluorescence peaks of the $(CuInZn)S_2$ material are both signifi-cantly blue shifted from those of the $CuInS_2$ quantum dots formed from the same In–S complex solution, consistent with the expected optical properties for quaternary alloy quantum dots.[61,62] Additionally, the level of fluorescence is significantly improved compared relative to the $CuInS_2$ quantum dots, but was still not able to match the improved peak intensity shown by the 'core/shell' type particles which had zinc acetate added after the formation of the $CuInS_2$ core. This indicates that adding zinc with copper does in fact produce an intimately mixed quaternary alloy, whereas adding zinc after the initial $CuInS_2$ quantum dots are formed produces a more core/shell type morphology.

Fig. 7(a) shows an HRTEM phase contrast image of a representative $(CuInZn)S_2$ nanocrystal from the sol whose optical properties are shown in Fig. 6. The particles appear to

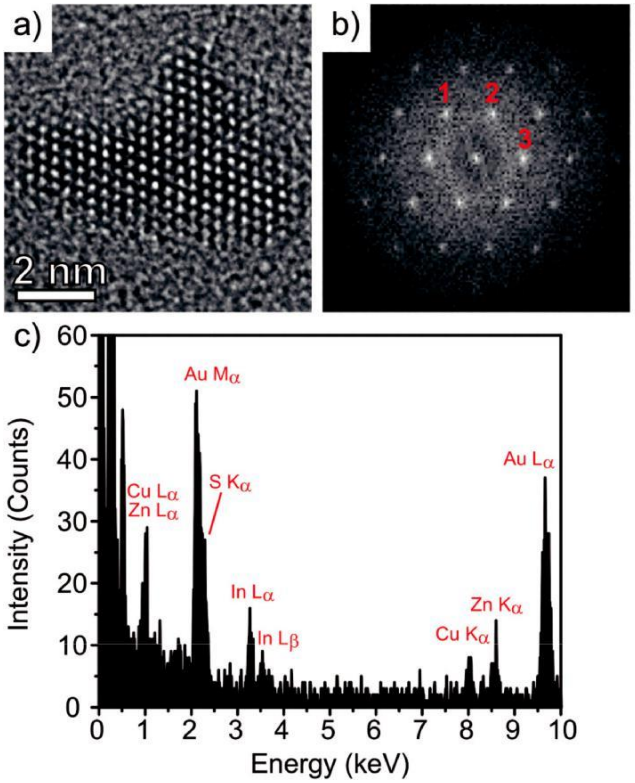

Fig. 7 (a) HRTEM phase contrast image and (b) corresponding FFT of a representative 5 nm (CuInZn)S_2 nanocrystal viewed along the [021$^-$] projection. Lattice fitting of planes indicated in the FFT are reported in Table S4.† (c) Representative STEM-XEDS spectrum showing the co-existence of Cu, In, S, and Zn within the single nanoparticle.

be ~5 nm in diameter and have a more irregular shape as compared to the corresponding $CuInS_2$ and $CuInS_2$/ZnS core/ shell particles. The photoluminescence peak at 575 nm is blue-shifted in comparison to other reports for 4–5 nm (CuInZn)S_2 nanocrystals with a nominal 1 : 1 : 1 stoichiometry of Cu : In : Zn cations. However, the cationic ratios measured using SEM-EDS was 1.84 ± 0.13 for Cu/In and 2.07 ± 0.14 for Cu/Zn. Similar to the core/shell nanocrystals, the Cu/In ratio is significantly increased with the incorporation of Zn as compared to the $CuInS_2$ core-only material. Jiang et al. have reported a significant blue-shift in the optical properties for (CuInZn)S_2 nanocrystals having a small indium content rela-tive to zinc.[19] The low indium content in addition to high zinc content in the alloy sample may play a dominant role in determining the optical properties as opposed to size quanti-zation in this case. Fig. 7(b) shows the corresponding FFT for the particle imaged on Fig. 7(a) which matches well to the [021] projection of the chalcopyrite phase (see lattice fringe fitting in Table S4†). A STEM-XEDS spectrum acquired from a single nanoparticle is shown in Fig. 7(c) and confirms that copper, indium, zinc, and sulfur all co-exist in a single particle. No separate nucleation of $Cu_{2-x}S$, In_2S_3, or ZnS nanocrystals was detected in our electron microscopy analyses.

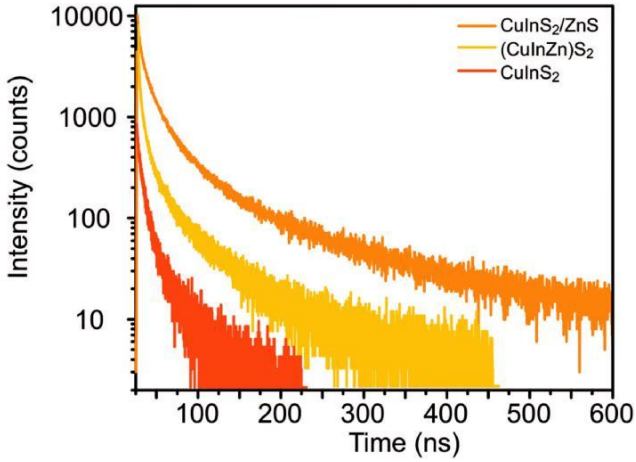

Fig. 8 Time resolved photoluminescence decay curves for the $CuInS_2$ core nanocrystals only, the (CuInZn)S_2 quaternary alloy and the $CuInS_2$/ ZnS core/shell nanocrystals.

This proposition of core/shell formation versus quaternary alloy formation is further verified through photoluminescence lifetime measurements of core $CuInS_2$, alloy (CuInZn)S_2, and core/shell $CuInS_2$/ZnS nanocrystals, as shown in Fig. 8. $CuInS_2$ particles typically have two decay lifetimes; the first, a short lifetime (~10–50 ns) and second longer lifetime (~100–500 ns), have been assigned to non-radiative and radiative decay processes, respectively.[9,10] Because our $CuInS_2$ core-only nano-crystals have poor photoluminescence characteristics, overall shorter lifetimes of 2.4 ns and 13.9 ns for these two processes were observed. The time constants increase slightly to 2.8 ns and 31 ns, respectively, for the (CuInZn)S_2 quaternary alloy nanocrystals. Both time constants increase markedly to 9.4 ns and 74.5 ns respectively, upon incubation of $CuInS_2$ in the zinc acetate containing solution to form $CuInS_2$/ZnS core/shell nanocrystals. In the case of the (CuInZn)S_2 alloyed nanocrys-tals, the increase in the decay emission is attributed to a slight passivation of donor defects within the crystal lattice.[61] The substantial increase in the radiative decay lifetime for the $CuInS_2$/ZnS core/shell type quantum dots is a typical result of increased surface passivation upon growth of a shell onto core nanocrystals.[10]

To demonstrate that our biomineralized $CuInS_2$/ZnS core/ shell nanocrystals could be effective for bio-labeling, the as-synthesized quantum dots were conjugated to IgG antibodies using EDC/NHS cross-linkers, which then bind to the epidermal growth factor receptor (EGFR) of the THP-1 leukemia cells. THP-1 is an established cell line used for biomarker detection in cancer and contains the target receptor of interest, namely EGFR.[63,64] Fig. 9(a) shows a confocal image of THP-1 cells incubated with $CuInS_2$/ZnS nanocrystals that had not yet been conjugated to anti-EGFR antibody. The red signal indicates fluorescence from the $CuInS_2$/ZnS quantum dots, which is even across the sample, confirming no site-specific fluorescence inside the cells. In contrast, Fig. 9(b) shows a confocal image of THP-1 cells after 1 h of incubation with $CuInS_2$/ZnS quantum

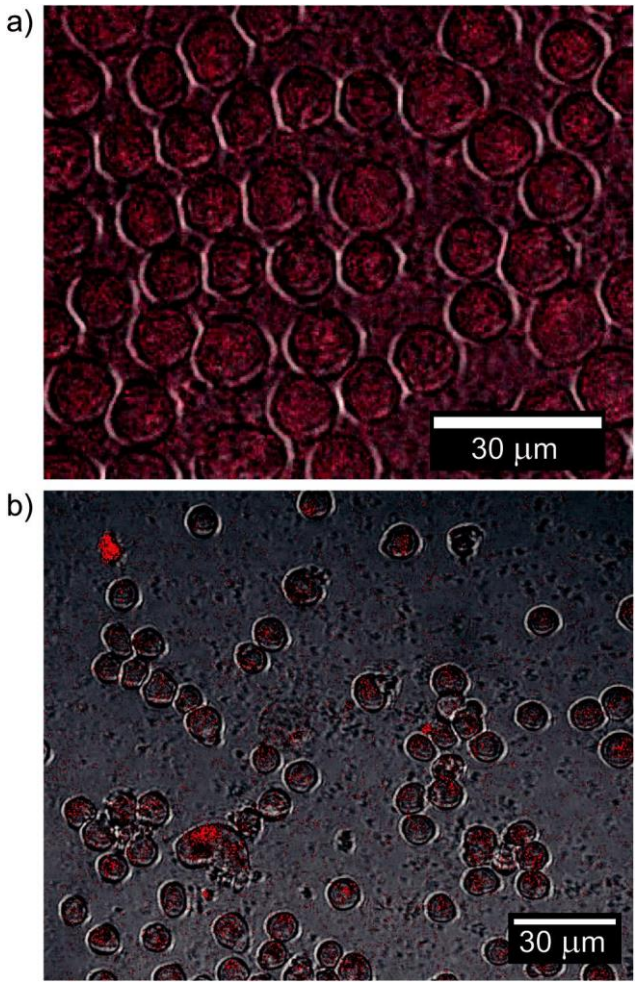

Fig. 9 Light optical confocal microscope images of THP-1 cells (a) incubated in solution with $CuInS_2$/ZnS quantum dots with no IgG antibody tagging, and (b) tagged with $CuInS_2$/ZnS quantum dots, bio-conjugated to an IgG antibody. The red coloration corresponds to quantum dot fluorescence, and is only site specific when the IgG antibody on the THP-1 leukemia cells are conjugated to the $CuInS_2$/ZnS nanocrystals.

dots tagged with IgG. The cells were washed twice prior to imaging in the confocal light-optical microscope to remove any unbound quantum dots. The fluorescence from the $CuInS_2$/ZnS quantum dot-IgG conjugates is localized to patches on the cell surface; a similar pattern of EGFR clustering at the cell surface has been described before due to the dimer-dependent acti-vation of EGFR.[65,66] The absence of site specific fluorescence in Fig. 9(a) confirms that the $CuInS_2$/ZnS quantum dots were not taken into to cells using already present endocytosis or phago-cytosis pathways, which has been previously reported for small nanocrystals.[67,68] In order to monitor the toxicity of quantum dots, a Trypan blue assay was utilized to determine the percent-age of dead THP-1 cells after incubation with the $CuInS_2$/ZnS quantum dot solution. Over a period of 6 h, the percentage of living cells remained at an average of 95.5% ± 2.6%, demon-strating that the quantum dots have little or no adverse toxic effect on the target THP-1 cells.

Discussion

The biomineralization of $CuInS_2$ or $(CuInZn)S_2$ nanocrystals requires a slightly more complex approach than the straight-forward direct biomineralization from buffered solutions of metal salt, L-cysteine and CSE demonstrated for $Cu_{2-x}S$ and ZnS herein, and for PbS and CdS in our previous work.[34,35] These latter materials will directly form a metal sulfide solid upon reaction with the reactive sulfur, likely H_2S, formed by the enzymatic turnover of L-cysteine by the putative cystathio-nine γ-lyase class CSE enzyme.[28] In contrast, reaction with indium nitrate forms a relatively stable species with a charac-teristic absorption peak at 290 nm, which has previously been identified as a molecular cluster of indium and sulfur,[46] rather than bulk or nanocrystalline In_2S_3. A similar result is obtained upon addition of Na_2S to a mixture of indium nitrate with L-cysteine, whereas a bulk precipitate of In_2S_3 likely combined with indium hydroxide is formed in the absence of L-cysteine. Thus, it appears that L-cysteine acts to stabilize these clusters. Formation of $CuInS_2$ or $(CuInZn)S_2$ nanocrystals can be initiated by reaction of copper acetate, or copper acetate and zinc acetate, in solutions containing these biologically gener-ated clusters containing indium and sulfur.

The biomineralized $CuInS_2$ and $(CuInZn)S_2$ nanocrystals produced are within the quantum confined size range and exhibit crystal structures, lattice parameters and optical absor-bance maxima positions that are equivalent to their chemically synthesized counterpart materials. Single particle XEDS ana-lysis confirms the co-existence of the constituent elements within individual particles. As further verification, a chemical aqueous synthesis of $CuInS_2$ prepared via the addition of reac-tive Na_2S to a solution of copper acetate, indium chloride and L-cysteine templating agent,[22] forms nanocrystals with optical properties analogous to our purely biomineralized materials. In the chemical synthesis case, Na_2S acts as the reactive sulfur source in place of the enzymatic generation of H_2S by CSE. Thus, our biomineralization approach is capable of producing biocompatible quantum dots in the aqueous phase under ambient conditions. Unfortunately, the photoluminescence characteristics of these 'as-generated' nanoparticles are quite low, indicative of poor surface passivation in the aqueous phase due to the low synthesis temperature employed.

Photoluminescence from $CuInS_2$ and $(CuInZn)S_2$ nanocrys-tals is thought to occur from intrinsic defects in the crystal structure, although the exact decay pathway is still a matter of debate.[9] This leads to relatively wide peak widths, as indicated by large full-width-half-maxima (FWHM) of ~300 meV, even with size selective precipitation, and a large Stokes' shift of ~450 meV.[10,50,69] Our aqueous phase, room temperature bio-synthesized nanocrystals display similar FWHM values of 300, 590 and 430 meV, and a Stokes shift of 400, 300 and 650 meV, for the $CuInS_2$, (CuInZn)S and $CuInS_2$/ZnS, particle variants respectively. Our Stokes shift values are slightly larger than those reported for analogous chemically prepared materials (cf. ~400 meV for $CuInS_2$/ZnS quantum dots chemically syn-thesized in the aqueous phase at 95 °C).[22] The $(CuInZn)S_2$

quaternary alloy nanocrystals have a significantly higher FWHM, which is to be expected based on their highly irregular shapes.[19]

The low photoluminescence intensity of the as-synthesized $CuInS_2$ nanocrystals is most likely due to the presence of surface trap states that lead to non-radiative recombination pathways,[11] and cause the short lifetimes reported in Fig. 6. The improvement in both photoluminescence intensity and lifetimes for the $(CuInZn)S_2$ alloy nanocrystals relative to $CuInS_2$ is most likely due to passivation of defects within the crystal lattice. Further improvement in photoluminescence and lifetimes is achieved through passivation of surface defects through the growth of a ZnS shell on the $CuInS_2$ nano-crystals. While from electron microscopy studies we cannot completely exclude the possibility of some limited zinc diffusion into the $CuInS_2$ particles rather than solely forming a ZnS overlayer, shell growth is indicated by the substantial improvement in photoluminescence intensity and lifetime when compared to the corresponding fully alloyed $(CuInZn)S_2$ particles.

$CuInS_2$ and $(CuInZn)S_2$ nanocrystals are typically formed at high temperature in an organic phase and must be phase transferred and stabilized in the aqueous phase prior to appli-cation as a fluorescent marker in biological systems.[11,12] While this chemical approach leads to high quality materials in terms of quantum yield, it is an energy intensive and more complex synthesis route which is intrinsically far away from the generally desirable ethos of green production of materials. In contrast, the direct biomineralization approach demon-strated in this paper results in the fabrication of stable quantum confined nanocrystals directly in the aqueous phase at room temperature.

Bioimaging applications generally require stable, aqueous phase nanocrystals that can be functionalized with a biological marker, such as an antibody. While $CuInS_2$ and $(CuInZn)S_2$ nanocrystals are typically chemically synthesized in the organic phase, they then need to be transferred into water using ligand exchange, or more commonly, encapsulation in a polymer shell, such as PEG.[13] Notably, any phase transfer procedure typically reduces the quantum yield,[12,13] while ligand exchange also reduces the stability of the quantum dots.[6] Polymer encapsula-tion also inevitably results in nanocrystals which are much larger than their initial nominal size.[2] Our biomineralized quantum dots have the advantage of being synthesized in bio-logically relevant aqueous buffers, and have high stability while still retaining an ultra-small size. They do not require any additional processing steps after synthesis and can be conju-gated to antibodies directly from the synthesis solution without adversely affecting cell-surface binding properties.

The primary drawback of the biomineralization approach is the relatively low photoluminescence intensity displayed by our nanocrystals even after ZnS capping, when compared to those fabricated at high temperature in the organic phase via traditional chemical routes.[13,61] This is most likely due to the combination of the aqueous solvent and low temperature syn-thesis conditions employed. As noted, the quantum yield of chemically synthesized materials is reduced significantly upon phase transfer to the aqueous phase due to relatively poor capping by the aqueous stabilizing ligands.[12,13] While some groups have reported quantum yields of up to 38% for aqueous synthesized $CuInS_2$/ZnS core/shell nanocrystals, these alternative chemical synthesis routes utilize elevated tempera-tures and/or pressure.[22] Growth at lower temperatures likely leads to a greater intrinsic defect population in the particles. However, this must be placed in context with the relative infancy of this enzymatic biomineralization approach to func-tional nanomaterial synthesis when compared to the more tra-ditional routes. We anticipate that further developments of these embryonic biomineralized synthesis protocols will occur over time and lead to higher quality materials, just as they have over the past two decades for the chemical synthesis protocols.

Conclusions

This work has unambiguously demonstrated the direct bio-mineralization of $CuInS_2$, $(CuInZn)S_2$, and $CuInS_2$/ZnS core/shell quantum dots in the aqueous phase using a single enzyme, namely CSE. The $CuInS_2$ and $(CuInZn)S_2$ alloy nanocrystals are formed using a two-step nucleation process; the first step creates soluble In-S complexes stabilized by L-cysteine, while the second step immediately forms $CuInS_2$ or $(CuInZn)S_2$ nanoparticles following the addition of the corresponding non-indium precursor(s). The CSE can also be utilized for sub-sequent ZnS shell growth on $CuInS_2$, and is achieved by adding zinc acetate to the preformed $CuInS_2$ quantum dots, resulting in a dramatic improvement in their photo-luminescence performance. The resultant $CuInS_2$/ZnS particles can be successfully conjugated to an IgG antibody using EDC/ NHS cross-linkers and then utilized for the specific tagging of EGFR receptors on THP-1 leukemia cells and used for their subsequent visualization in confocal fluorescence optical microscopy experiments.

Acknowledgements

This material is based upon work supported by the National Science Foundation under the EFRI-PSBR program, Grant No. 1332349. We thank Dr Angela Brown of the Department of Chemical Engineering for use of the fluorometer. We would also like the thank Evan Koufus of the Brown lab for culturing THP-1 cells, helping plan the cell tagging experiments, and performing confocal optical microscopy. We thank Dr Damien Thévenin of the Department of Chemistry for use of the fluorometer with TCSPC controller for performing lifetime measurements.

References

1 J. Zhou, Y. Yang and C. Zhang, Chem. Rev., 2015, 115, 11669–11717.

2 N. Erathodiyil and J. Y. Ying, Acc. Chem. Res., 2011, 44, 925–935.
3 N. Hildebrandt, C. M. Spillmann, W. R. Algar, T. Pons, M. H. Stewart, E. Oh, K. Susumu, S. A. Díaz, J. B. Delehanty and I. L. Medintz, Chem. Rev., 2016, 117, 536–711.
4 Y. Zheng, S. Gao and J. Y. Ying, Adv. Mater., 2007, 19, 376–380.
5 X. Wu, H. Liu, J. Liu, K. N. Haley, J. A. Treadway, J. P. Larson, N. Ge, F. Peale and M. P. Bruchez, Nat. Biotechnol., 2003, 21, 41–46.
6 W. J. Parak, D. Gerion, T. Pellegrino, D. Zanchet, C. Micheel, S. C. Williams, R. Boudreau, M. A. Le Gros, C. A. Larabell and A. P. Alivisatos, Nanotechnology, 2003, 14, R15.
7 G. Guo, W. Liu, J. Liang, Z. He, H. Xu and X. Yang, Mater. Lett., 2007, 61, 1641–1644.
8 S. Chang, Y. Dai, B. Kang, W. Han, L. Mao and D. Chen, Toxicol. Lett., 2009, 188, 104–111.
9 A. D. Leach and J. E. Macdonald, J. Phys. Chem. Lett., 2016, 7, 572–583.
10 A. C. Berends, F. T. Rabouw, F. C. Spoor, E. Bladt, F. C. Grozema, A. J. Houtepen, L. D. Siebbeles and C. de Mello Donegá, J. Phys. Chem. Lett., 2016, 7, 3503–3509.
11 L. Li, T. J. Daou, I. Texier, T. T. Kim Chi, N. Q. Liem and P. Reiss, Chem. Mater., 2009, 21, 2422–2429.
12 T. Pons, E. Pic, N. Lequeux, E. Cassette, L. Bezdetnaya, F. Guillemin, F. Marchal and B. Dubertret, ACS Nano, 2010, 4, 2531–2538.
13 D. Deng, Y. Chen, J. Cao, J. Tian, Z. Qian, S. Achilefu and Y. Gu, Chem. Mater., 2012, 24, 3029–3037.
14 K. N. Thakkar, S. S. Mhatre and R. Y. Parikh, Nanomedicine, 2010, 6, 257–262.
15 N. Gaponik and A. L. Rogach, Semiconductor Nanocrystal Quantum Dots, ed. A. L. Rogach, Springer, 2008, p. 73–99.
16 S. Liu, H. Zhang, Y. Qiao and X. Su, RSC Adv., 2012, 2, 819–825.
17 A. Arshad, H. Chen, X. Bai, S. Xu and L. Wang, Chin. J. Chem., 2016, 34, 576–582.
18 X. Gao, Z. Liu, Z. Lin and X. Su, Analyst, 2014, 139, 831– 836.
19 T. Jiang, J. Song, H. Wang, X. Ye, H. Wang, W. Zhang, M. Yang, R. Xia, L. Zhu and X. Xu, J. Mater. Chem. B, 2015, 3, 2402–2410.
20 Y. Xu, T. Chen, X. Hu, W. Jiang, L. Wang, W. Jiang and J. Liu, J. Colloid Interface Sci., 2017, 496, 479–486.
21 W. Xiong, G. Yang, X. Wu and J. Zhu, ACS Appl. Mater. Interfaces, 2013, 5, 8210–8216.
22 Y. Chen, S. Li, L. Huang and D. Pan, Inorg. Chem., 2013, 52, 7819–7821.
23 M. Wang, X. Liu, C. Cao and C. Shi, RSC Adv., 2012, 2, 2666–2670.
24 S. Mann, Biomineralization: principles and concepts in bioinorganic materials chemistry, Oxford University Press on Demand, 2001.
25 S. Tom, H. Jin, K. Heo and S. Lee, Nanoscale, 2016, 8, 15696–15701.
26 C. Xu, Y. Wang, C. Zhang, Y. Jia, Y. Luo and X. Gao, Nanoscale, 2017, 9, 4620–4628.
27 Y. S. Nam, H. Park, A. P. Magyar, D. S. Yun, T. S. Pollom and A. M. Belcher, Nanoscale, 2012, 4, 3405–3409.
28 R. Dunleavy, L. Lu, C. J. Kiely, S. McIntosh and B. W. Berger, Proc. Natl. Acad. Sci. USA, 2016, 113, 5275–5280.
29 Z. Yang, L. Lu, C. J. Kiely, B. W. Berger and S. McIntosh, ACS Appl. Mater. Interfaces, 2017, 9, 13430–13439.
30 M. Grabolle, M. Spieles, V. Lesnyak, N. Gaponik, A. Eychmüller and U. Resch-Genger, Anal. Chem., 2009, 81, 6285–6294.
31 D. A. East, M. Todd and I. J. Bruce, Quantum Dots: Applications in Biology, Springer, 2014, pp. 67–83.
32 L. P. Chandler, C. E. Chandler, M. Hosang and E. M. Shooter, J. Biol. Chem., 1985, 260, 3360–3367.
33 H. Li, M. Li, W. Y. Shih, P. I. Lelkes and W. Shih, J. Nanosci. Nanotechnol., 2011, 11, 3543–3551.
34 L. C. Spangler, L. Lu, C. J. Kiely, B. W. Berger and S. McIntosh, J. Mater. Chem. A, 2016, 4, 6107–6115.
35 Z. Yang, L. Lu, V. F. Berard, Q. He, C. J. Kiely, B. W. Berger and S. McIntosh, Green Chem., 2015, 17, 3775–3782.
36 Z. Yang, L. Lu, C. J. Kiely, B. W. Berger and S. McIntosh, Ind. Eng. Chem. Res., 2016, 55, 11235–11244.
37 R. H. Kore, J. S. Kulkarni and S. K. Haram, Chem. Mater., 2001, 13, 1789–1793.
38 X. Liu, B. Li, F. Fu, K. Xu, R. Zou, Q. Wang, B. Zhang, Z. Chen and J. Hu, Dalton Trans., 2014, 43, 11709–11715.
39 S. Prasanth, D. R. Raj, T. Vineeshkumar, R. K. Thomas and C. Sudarsanakumar, RSC Adv., 2016, 6, 58288–58295.
40 I. Kriegel, C. Jiang, J. Rodríguez-Fernández, R. D. Schaller, D. V. Talapin, E. Da Como and J. Feldmann, J. Am. Chem. Soc., 2012, 134, 1583–1590.
41 Y. Wu, C. Wadia, W. Ma, B. Sadtler and A. P. Alivisatos, Nano Lett., 2008, 8, 2551–2555.
42 P. Kumta, P. P. Phule and S. H. Risbud, Mater. Lett., 1987, 5, 401–404.
43 M. V. Ivanchenko, O. E. Rayevska, O. L. Stroyuk and S. Y. Kuchmiy, Mater. Res. Soc. Symp. Proc., 2013, 1617, 163–169.
44 P. V. Kamat, N. M. Dimitrijevic and R. W. Fessenden, J. Phys. Chem., 1988, 92, 2324–2329.
45 Y. Nosaka, N. Ohta and H. Miyama, J. Phys. Chem., 1990, 94, 3753.
46 D. K. Nagesha, X. Liang, A. A. Mamedov, G. Gainer, M. A. Eastman, M. Giersig, J. Song, T. Ni and N. A. Kotov, J. Phys. Chem. B, 2001, 105, 7490–7498.
47 C. Lokhande, Mater. Chem. Phys., 1991, 27, 1–43.
48 D. So and G. Konstantatos, Chem. Mater., 2015, 27, 8424–8432.
49 W. Van Der Stam, A. C. Berends, F. T. Rabouw, T. Willhammar, X. Ke, J. D. Meeldijk, S. Bals and C. de Mello Donega, Chem. Mater., 2015, 27, 621–628.
50 H. Zhong, Y. Zhou, M. Ye, Y. He, J. Ye, C. He, C. Yang and Y. Li, Chem. Mater., 2008, 20, 6434–6443.
51 D. H. Jara, S. J. Yoon, K. G. Stamplecoskie and P. V. Kamat, Chem. Mater., 2014, 26, 7221–7228.

52 Y. Kim, S. Ahn, K. Chung, Y. Cho and C. Choi, J. Mater. Chem., 2012, 22, 1516–1520.
53 M. Uehara, K. Watanabe, Y. Tajiri, H. Nakamura and H. Maeda, J. Chem. Phys., 2008, 129, 134709.
54 X. Wang and M. T. Swihart, Chem. Mater., 2015, 27, 1786–1791.
55 L. Li, A. Pandey, D. J. Werder, B. P. Khanal, J. M. Pietryga and V. I. Klimov, J. Am. Chem. Soc., 2011, 133, 1176–1179.
56 A. Ghatak, G. H. Debnath, M. Mandal and P. Mukherjee, RSC Adv., 2015, 5, 32920–32932.
57 N. Kumbhojkar, V. Nikesh, A. Kshirsagar and S. Mahamuni, J. Appl. Phys., 2000, 88, 6260–6264.
58 L. S. Li, N. Pradhan, Y. Wang and X. Peng, Nano Lett., 2004, 4, 2261–2264.
59 S. Liu, H. Zhang, Y. Qiao and X. Su, RSC Adv., 2012, 2, 819–825.
60 J. Zhang, R. Xie and W. Yang, Chem. Mater., 2011, 23, 3357–3361.
61 L. De Trizio, M. Prato, A. Genovese, A. Casu, M. Povia, R. Simonutti, M. J. Alcocer, C. D'Andrea, F. Tassone and L. Manna, Chem. Mater., 2012, 24, 2400–2406.
62 Q. A. Akkerman, A. Genovese, C. George, M. Prato, I. Moreels, A. Casu, S. Marras, A. Curcio, A. Scarpellini and T. Pellegrino, ACS Nano, 2015, 9, 521–531.
63 S. Tsuchiya, M. Yamabe, Y. Yamaguchi, Y. Kobayashi, T. Konno and K. Tada, Int. J. Cancer, 1980, 26, 171–176.
64 B. Mograbi, N. Rochet, V. Imbert, I. Bourget, R. Bocciardi, C. Emiliozzi and B. Rossi, Eur. Cytokine Network, 1997, 8, 73–81.
65 S. Choi, J. Mendrola and M. Lemmon, Oncogene, 2007, 26, 1567–1576.
66 J. Ichinose, M. Murata, T. Yanagida and Y. Sako, Biochem. Biophys. Res. Commun., 2004, 324, 1143–1149.
67 W. J. Parak, R. Boudreau, M. Le Gros, D. Gerion, D. Zanchet, C. M. Micheel, S. C. Williams, A. P. Alivisatos and C. Larabell, Adv. Mater., 2002, 14, 882–885.
68 N. Feliu, J. Hühn, M. V. Zyuzin, S. Ashraf, D. Valdeperez, A. Masood, A. H. Said, A. Escudero, B. Pelaz and E. Gonzalez, Sci. Total Environ., 2016, 568, 819–828.
69 H. Zhong, S. S. Lo, T. Mirkovic, Y. Li, Y. Ding, Y. Li and G. D. Scholes, ACS Nano, 2010, 4, 5253–5262.